Title

Allosteric regulation of Na/Ca exchange current by cytosolic Ca in intact cardiac myocytes.

Journal

The Journal of general physiology, 117(2)

ISSN

0022-1295

Authors

Weber, CR
Ginsburg, KS
Philipson, KD
et al.

Publication Date

2001-02-01

DOI

10.1085/jgp.117.2.119

Peer reviewed

Allosteric Regulation of Na/Ca Exchange Current by Cytosolic Ca in Intact Cardiac Myocytes

Christopher R. Weber,* Kenneth S. Ginsburg,* Kenneth D. Philipson,‡
Thomas R. Shannon,* and Donald M. Bers*

From the *Department of Physiology, Loyola University Chicago, Stritch School of Medicine, Maywood, Illinois 60153; and ‡Cardiovascular Research Lab, University of California Los Angeles School of Medicine, Los Angeles, California 90095

ABSTRACT The cardiac sarcolemmal Na-Ca exchanger (NCX) is allosterically regulated by $[Ca]_i$ such that when $[Ca]_i$ is low, NCX current (I_{NCX}) deactivates. In this study, we used membrane potential (E_m) and I_{NCX} to control Ca entry into and Ca efflux from intact cardiac myocytes to investigate whether this allosteric regulation (Ca activation) occurs with $[Ca]_i$ in the physiological range. In the absence of Ca activation, the electrochemical effect of increasing $[Ca]_i$ would be to increase inward I_{NCX} (Ca efflux) and to decrease outward I_{NCX}. On the other hand, Ca activation would increase I_{NCX} in both directions. Thus, we attributed $[Ca]_i$-dependent increases in outward I_{NCX} to allosteric regulation. Ca activation of I_{NCX} was observed in ferret myocytes but not in wild-type mouse myocytes, suggesting that Ca regulation of NCX may be species dependent. We also studied transgenic mouse myocytes overexpressing either normal canine NCX or this same canine NCX lacking Ca regulation (Δ680–685). Animals with the normal canine NCX transgene showed Ca activation, whereas animals with the mutant transgene did not, confirming the role of this region in the process. In native ferret cells and in mice with expressed canine NCX, allosteric regulation by Ca occurs under physiological conditions (K_{mCaAct} = 125 ± 16 nM SEM ≈ resting $[Ca]_i$). This, along with the observation that no delay was observed between measured $[Ca]_i$ and activation of I_{NCX} under our conditions, suggests that beat to beat changes in NCX function can occur in vivo. These changes in the I_{NCX} activation state may influence SR Ca load and resting $[Ca]_i$, helping to fine tune Ca influx and efflux from cells under both normal and pathophysiological conditions. Our failure to observe Ca activation in mouse myocytes may be due to either the extent of Ca regulation or to a difference in K_{mCaAct} from other species. Model predictions for Ca activation, on which our estimates of K_{mCaAct} are based, confirm that Ca activation strongly influences outward I_{NCX}, explaining why it increases rather than declines with increasing $[Ca]_i$.

KEY WORDS: Na/Ca exchanger • cardiac electrophysiology • ferret • mouse • dog

INTRODUCTION

The cardiac sarcolemmal Na/Ca exchanger (NCX)[1] is a reversible transporter that exchanges three (Reeves and Hale, 1984; Kimura et al., 1987) or possibly four (Fujioka et al., 2000) Na for one Ca. Outward Na/Ca exchange current (I_{NCX}), or Ca influx, is electrochemically favored by low $[Ca]_i$, high $[Na]_i$, and depolarized membrane potentials. Inward I_{NCX}, or Ca efflux, is favored by the opposite conditions (Mullins, 1979; Bers, 1991). In addition to the electrochemical potential, which sets the direction of I_{NCX}, NCX is allosterically regulated by $[Ca]_i$ such that when $[Ca]_i$ is low, I_{NCX} deactivates (Miura and Kimura, 1989). NCX proteins in this state do not contribute to I_{NCX}. Increasing $[Ca]_i$ can activate NCX, allowing I_{NCX} to flow.

Allosteric Ca binds at two acidic regions in the large cytoplasmic loop of the NCX, each containing three consecutive aspartic acid residues (D446–D448 and D498–D500; Matsuoka et al., 1995). The loop has been shown to bind Ca cooperatively ($n_{Hill} \approx 2$) with a $K_{1/2}$ ranging from 0.3 to 3 μM in vitro, depending on the concentration of Mg (0.2–5 mM, respectively; Levitsky et al., 1994). α-Chymotrypsin treatment eliminates Ca activation for outward (Hilgemann, 1990; Hilgemann et al., 1992; Matsuoka et al., 1993) and inward I_{NCX} (Kappl and Hartung, 1996) in giant membrane patches. Attempts to measure the affinity for Ca to the activating site of the NCX have given disparate results in different experimental conditions.

Miura and Kimura (1989), using intracellular perfusion to control $[Ca]_i$, showed Ca-dependent activation of outward I_{NCX} in guinea pig myocytes. Outward I_{NCX} was fully activated at $[Ca]_i$ = 50 nM (below the normal resting [Ca] of ~100 nM). Fang et al. (1998) measured Ca activation (K_{mCaAct} = 44 nM, n_{Hill} = 1.6) of Na-dependent Ba influx in Chinese hamster ovary cells expressing bovine NCX, to assay I_{NCX}. Deletion of a large portion of the cytoplasmic loop (Δ241-680), which contains the putative Ca regulatory domain, eliminated

Address correspondence to Donald M. Bers, Ph.D., Department of Physiology, Loyola University Chicago, Stritch School of Medicine, 2160 South First Avenue, Maywood, IL 60153. Fax (708) 216-6308; E-mail: dbers@luc.edu

[1]*Abbreviations used in this paper:* I_{NCX}, NCX current; NCX, Na/Ca exchanger, WT, wild-type.

variations in Ba influx with changing $[Ca]_i$, supporting the study by Matsuoka et al. (1993). In contrast, Haworth and Goknur (1991) showed apparent activation of I_{NCX} at physiological $[Ca]_i$. Field stimulation of ^{22}Na-loaded rat myocyte suspensions resulted in increased Na pump–independent Na efflux. This suggests that the entry of physiologically relevant amounts of Ca through Ca channels can activate the NCX.

All measurements in giant excised patches so far have shown Ca-dependent regulation at physiological $[Ca]_i$. In giant patches from guinea pig myocytes, Ca activation of outward I_{NCX} was seen with K_{mCaAct} = 300–600 nM (Hilgemann et al., 1992). In patches from *Xenopus* oocytes expressing canine cardiac NCX, mutations of various residues within and near to the two acidic Ca regulatory regions increase K_{mCaAct} from 0.4 μM to between 1.1 and 1.8 μM (Matsuoka et al., 1995). Approximately 180 amino acids downstream of the two acidic DDD segments, amino acids 680–685 (IIEESY in canine NCX1) are also important for Ca activation. Giant patches from transgenic mouse myocytes overexpressing a deletion mutant of these six residues (Δ680-685) show outward I_{NCX}, which is nearly fully activated at all $[Ca]_i$ (Maxwell et al., 1999).

In this study, we took advantage of the electrogenicity of the NCX to control Ca entry into and Ca efflux from intact cardiac myocytes to measure the effects of changing $[Ca]_i$ on I_{NCX}. Using solutions that were selective for I_{NCX}, we voltage-clamped single cells at +100 mV to bring Ca into the cell through outward I_{NCX} and at −100 mV to bring Ca out of the cell through inward I_{NCX}. By varying the depolarization duty factor ($t_{+100\ mV}$/total t), we were able to directly control $[Ca]_i$, and at the same time observe the effects of changing $[Ca]_i$ on I_{NCX}. This study differs from earlier studies in that $[Ca]_i$ was dynamically controlled by a physiological process rather than being artificially clamped to particular values by exogenous buffering. Advantages of our study are as follows: measurements were made in the normal cellular environment; and dynamic changes in $[Ca]_i$ in the physiological range were examined.

We observed clear Ca activation of I_{NCX} in ferret myocytes, but did not detect appreciable regulation in wild-type (WT) mouse myocytes using the same protocols (in contrast to Maxwell et al., 1999). No delay was observed between the rise in $[Ca]_i$ and activation of I_{NCX}. We also studied mouse myocytes overexpressing normal canine NCX (Adachi-Akahane et al., 1997) and mouse myocytes overexpressing this same canine NCX lacking the Ca regulatory domain Δ680-685 (Maxwell et al., 1999). Animals with the normal canine NCX transgene showed Ca activation, whereas animals with the mutant transgene did not. Some of the results shown in this article were presented in abstract form (Weber et al., 1999, 2000).

MATERIALS AND METHODS

Cell Preparation

Cells were isolated using approved methods. Ferrets were anesthetized with sodium pentobarbital (50 mg/kg IP). Hearts were excised, rinsed in ice-cold 0 mM Ca Tyrode's solution, and placed on a Langendorf apparatus for retrograde constant flow (30–36 ml/min) perfusion of the coronary vasculature via the aorta at 37°C. The heart was perfused for 5 min with 0-mM Ca Tyrode's solution, after which an otherwise identical solution containing filtered collagenase (Yakult Corp. or Boehringer) as well as 10 μM Ca was perfused. When the heart was slightly flaccid to touch, enzyme activity was stopped by perfusion with 0-mM Ca Tyrode's solution containing BSA. Ventricles were removed from the apparatus, cut into ~2-mm^3 size pieces, and gently triturated. After washing in Ca-free solution at room temperature, cells were placed on laminin-coated perfusion chambers for recording. Cells were used within 6 h of isolation.

The preparation of mouse myocytes was modified to reduce the risk of ischemic damage to the hearts. Mice were anesthetized by inhalation with a mixture of 5% isoflurane and 95% O_2. Each mouse was tracheotomized and mechanically ventilated. Upon opening the chest cavity, we injected cold high K cardioplegia solution into the vena cava and quickly excised the heart, which was subsequently transferred to a gravity-driven (80 mmHg) apparatus for perfusion at 37°C (flow rate ≈ 3 ml/min) and treated as above.

Fluorescent Measurement of $[Ca]_i$

Perfusion chambers were mounted on a Nikon TMD epifluorescence microscope. Cells were loaded with 10 μM indo-1 AM, applied externally for 22 min at 23°C, or 100 μM K indo-1, applied through the pipet, in perforated patch and ruptured patch experiments, respectively. We allowed indo-1 AM to deesterify for 20 min before proceeding with $[Ca]_i$ measurements. Cells were excited at 365 ± 5 nm using a 75-W xenon arc lamp via epiillumination, and emitted fluorescence (405 ± 10 nm and 485 ± 10 nm) was recorded using photometers (PTI Corp.). For indo-1 AM experiments, a linear regression of autofluorescence at each wavelength versus two-dimensionally projected cell surface area for 10 unloaded cells of the same preparation was used to predict the background to be subtracted from the loaded signal for each cell studied, according to the particular cell's size. For K indo-1 experiments, the autofluorescence of the cell being studied was always recorded before patch rupture. The ratio (R) of emitted fluorescence at 405 nm to emitted fluorescence at 485 nm was converted to $[Ca]_i$ using the Grynkiewicz et al. (1985) equation: $[Ca]_i = K_d\,\beta(R - R_{min})/(R_{max} - R)$. R_{min} (0.24), R_{max} (2.91), and β (4.17) were determined, and K_d was taken as 844 nm as described by Bassani et al. (1995). Cell contraction was apparent under visible light >650 nm provided by transillumination (which was deflected from the fluorescence detector pathway by a short pass dichroic mirror), and was simultaneously recorded using a video edge detection system. This served as an additional indicator of changes in $[Ca]_i$.

In most mouse myocyte experiments, we used fluo-3 AM, since we were able to attain better Ca signals than with indo-1 AM or K indo-1. 5 μM fluo-3 AM was loaded until fluorescence was three or more times background (up to ~45 min), and a comparable time was allowed for deesterification. In experiments using fluo-3, cells were excited at 480 ± 5 nm, and emission was recorded at 535 ± 20 nm. To convert nonratiometric signals into $[Ca]_i$, the following pseudoratio equation was used (Cheng et al., 1993): $[Ca]_i = K_d \cdot R/((K_d/[Ca]_{rest}) + 1 - R)$. R was taken as the emitted fluorescence divided by the resting emitted fluorescence, each

after background subtraction. $[Ca]_{rest}$ was taken as 100 nM, and K_d = 1,100 nM was used to calculate $[Ca]_i$. In several experiments with indo-1 AM, when an ideal calibration was not available, we also treated background subtracted indo-1 ratios using the pseudoratio method. There was no apparent qualitative or quantitative difference in results which could be attributed to the different indicator methods used.

Solutions for Electrophysiological Recording

To eliminate any contribution of the SR to Ca handling, cells were pretreated for 10 min with 0Ca/0Na Tyrode's solution containing (in mM): 0.001 thapsigargin, 10 caffeine, 140 LiCl, 6 KCl, 1 $MgCl_2$, 10 glucose, and 5 HEPES, pH 7.4 with LiOH. Patch electrodes (1–2 MΩ) were tip-dipped and backfilled with solution containing (in mM): 40 CsCl, 80 tetraethylammonium chloride (TEACl) 0.92 $MgCl_2$, 10 HEPES, 10 NaCl, 5 MgATP, 0.3 LiGTP, and 0.1 K indo-1; pH was set to 7.2 with CsOH and free [Mg] was ~0.5 mM. In some cases, we used aspartic acid and equimolar CsOH instead of the TEACl. For perforated patch experiments on cells loaded with indo-1 AM or fluo-3 AM, nucleotides and K indo-1 were omitted and 140 μg/ml amphotericin was added to the portion of solution used to backfill the electrodes. Cells were sealed in Tyrode's solution containing (in mM): 140 NaCl, 4 KCl, 10 glucose, 5 HEPES, and 1 $MgCl_2$, with pH set to 7.4 using NaOH. External Ca was 1 mM in mouse and 2 mM in ferret experiments. After electrical access to the interior of the cell was attained, the external solution was switched to Tyrode's solution containing 4 mM CsCl instead of KCl. To secure the best possible voltage control, series resistance was compensated to the extent possible. Additionally, we applied capacitance transient cancellation either during the recording or analytically.

To better isolate I_{NCX}, we also used a combination of drugs to block unwanted sarcolemmal currents (20 μM nifedipine to block L-type Ca current, 30 μM niflumic acid to block Ca activated Cl current, and 4 μM *N*-acetylstrophanthidin to block the Na/K ATPase). We did not specifically block $I_{Ca}(T)$; however, $I_{Ca}(T)$ has not been observed in ferret ventricular myocytes (Yuan and Bers, 1995). Further, any $I_{Ca}(T)$ activated on depolarization to +100 mV would support only a negligible Ca influx (since E_{rev} for Ca is near +100 mV) and would inactivate very quickly (Satin and Cribbs, 2000).

Protocols

We designed our voltage protocol (see Fig. 2 C, bottom) to control $[Ca]_i$ and measure I_{NCX} at the same time. At the beginning of each recording, and again before any repetition of the protocol, cells were held at −100 mV for 3 min or more, to promote inward I_{NCX} (Ca extrusion) such that cells were initialized to low $[Ca]_i$. Thereafter, repetitive pulses from −100 mV to +100 mV were applied to set the direction of I_{NCX}. Inward I_{NCX}, or Ca extrusion, was greatly favored at −100 mV, whereas the converse was true at +100 mV (positive to E_{NCX}). Usually, the duration of each pulse was 100 ms, but by varying the duty factor, it was possible to control $[Ca]_i$ more specifically and to observe corresponding changes in inward and outward I_{NCX} magnitudes. For example, with 100 ms at +100 mV and 200 ms at –100 mV in Fig. 2 C (bottom) the duty factor was 0.33. In the four myocyte types studied, I_{NCX} was recorded with increasing $[Ca]_i$, using alternating protocols like that shown in Fig. 2 C (bottom). The duty factor of the voltage protocol was chosen for each cell (0.25–0.67) to adjust net Ca entry into the cell in a range which would vary activation of I_{NCX} from minimal to maximal.

Qualification of Recorded Currents

To minimize any influence of leakage current, cells were selected where the resting current after initialization to low $[Ca]_i$ (above) was as low as possible. Under this condition, the state of activation for I_{NCX} and the driving force for inward I_{NCX} would both be minimized, and any residual inward current would be largely due to leak. I_{NCX} was taken as the current blocked by 10 mM Ni. In some cases, when it was not possible to apply Ni to the cell, the records were leak subtracted. For this purpose, we used the linear leak conductance (g_{leak}) determined from the inward resting current of the initialized cell to determine I_{leak} at all E_m ($I_{leak} = g_{leak} \cdot E_m$). This method of leak subtraction would define the initial I_{NCX} at the lowest resting $[Ca]_i$ to be zero. This is reasonable, since as cells rest at −100 mV during initialization to low $[Ca]_i$, I_{NCX} would be expected to approach equilibrium (where $E_m = E_{NCX} = 3E_{Na} - 2E_{Ca}$). Some inward I_{NCX} will flow to oppose any slow Ca entry into cells (Coulombe et al., 1989), so that in steady state it is not likely to reach zero. Despite this, the actual I_{NCX} we measured by Ni subtraction in cells initialized at resting $[Ca]_i$, was quite close to zero (see example in Fig. 2).

Simulations and Calculations

I_{NCX} was represented as the product of an electrochemical (ΔE) and an allosteric (Allo) factor. The ΔE factor is based on Equation IX-141 in Segel (1993), which describes the net reaction velocity (forward − backward) of the ping pong bi bi cyclic reaction scheme. We described the voltage dependence of the velocity in each direction using exponentials as defined by Mullins et al. (1979) and by Luo and Rudy (1994). Segel's equation was further simplified by assuming that the maximal flux is the same in both directions ($V_{maxr} = V_{maxf} = V_{max}$) and by making the approximation that the NCX dissociation constants for Ca_i and Na_i from catalytic sites are equivalent to the apparent K_m for Ca_i and Na_i transport by the NCX when other substrates are present at saturating concentrations (K_{mCai} and K_{mNai}). An instantaneous Hill equation for Ca binding to the regulatory site, and thus availability of the NCX, was used for the Allo factor as shown below:

$$I_{NCX} = (\text{Allo})(\Delta E)$$

$$\text{Allo} = \frac{1}{1 + \left(\frac{K_{mCaact}}{[Ca]_i}\right)^{n_{Hill}}}$$

$$\Delta E = \frac{V_{max}\left\{[Na]_i^3[Ca]_o e^{\left(\frac{\eta VF}{RT}\right)} - [Na]_o^3[Ca]_i e^{\left(\frac{(\eta-1)VF}{RT}\right)}\right\}}{\left\{\begin{array}{l} K_{mCa_o}[Na]_i^3 + K_{mNa_o}{}^3[Ca]_i + K_{mNa_i}{}^3[Ca]_o\left(1 + \frac{[Ca]_i}{K_{mCa_i}}\right) + \\ K_{mCa_i}[Na]_o^3\left(1 + \frac{[Na]_i^3}{K_{mNa_i}{}^3}\right) + [Na]_i{}^3[Ca]_o + [Na]_o^3[Ca]_i \end{array}\right\}\left\{1 + k_{sat} e^{\left(\frac{(\eta-1)VF}{RT}\right)}\right\}} \quad (1)$$

TABLE I

Fit Parameters

	Units	Ferret	WT mouse	Mouse + canine NCX	Mouse + Δ680-685
K_{mCaAct}	nM	125 ± 16	ND	152 and 394	ND
V_{max}	A/F	22.6 ± 5.3	4.4 ± 1.1	24.4 and 16.8	10.6 ± 4.1
$[Na]_i$	mM	7.2 ± 0.5	9.9 ± 0.7	10.4 and 14.4	15.5 ± 1.2.

Parameters (means ± SEM) for four cell types studied. K_{mCaAct} = not determined (ND) in cell types when including it did not improve the fits. Fixed parameters are listed in MATERIALS AND METHODS (see *Simulations and Calculations*).

The K_m values are the Na and Ca dissociation constants for intracellular (i) and extracellular (o) Na and Ca. η is the position of the energy barrier of the NCX in the membrane electric field, and k_{sat} is a factor that controls the saturation of I_{NCX} at negative potentials. K_{mCaAct} for each experiment was determined from curve fits of the I_{NCX} versus $[Ca]_i$ at +100 mV and −100 mV (Table I). During each voltage step, I_{NCX} and $[Ca]_i$ were averaged to obtain one data point for the fits, at a defined $[Ca]_i$ and voltage, resulting in 25–40 ($[Ca]_i$, I_{NCX}) pairs per experiment. For the fits, V_{max} and $[Na]_i$ were also allowed to vary between cells to account for cell to cell variation in I_{NCX} density and variations in the accuracy of $[Na]_i$ control by the pipet. Fixed parameters were as follows (and describe rabbit I_{NCX} data in Pogwizd et al., 1999): K_{mNao} = 87.5 mM (Kimura et al., 1987), K_{mNai} = 12.3 mM, K_{mCai} = 0.0036 mM (Hilgemann et al., 1991), K_{mCao} = 1.30 mM, k_{sat} = 0.27, η = 0.35, T = 23°C, and n_{Hill} = 2. K_{mNao}, K_{mCao}, K_{mCai}, and K_{mNai} satisfy a Haldane relationship (i.e., $V_{maxf}K_{mCai}K_{mNao}^3 = V_{maxr}K_{mNai}^3K_{mCao}$) with $V_{maxr} = V_{maxf} = V_{max}$. n_{Hill} = 2 may represent Ca binding to two anionic segments of the NCX1 cytoplasmic loop (Levitsky et al., 1994), and Fang et al. (1998) found n_{Hill} = 1.6. An F test (criterion *P* value < 0.05) on the residual error variance was used to determine if the above equation with the allosteric factor fit the I_{NCX} versus $[Ca]_i$ relationship better than the same equation without the allosteric factor. The test statistic applied to each data set was F = (SS1 − SS2)(DF1 − DF2)/(SS2/DF2), where SS1, SS2, DF1, and DF2 are the sum-of-squared errors and degrees of freedom (number of observations − number of free parameters) for the fit without (1) and the fit with (2) the allosteric factor (GraphPad Prism v3.00; GraphPad Software[http://www.graphpad.com]).

Additionally, ferret data were simulated using the above equation for I_{NCX} with a simple model for all other nonblocked sources of Ca flux (sarcolemmal Ca pump, Ca background leak current) but no SR (Fig. 1). Ca background leak current was taken as $I_{Cabkg} = G_{Cabkg}(E_m - E_{Ca})$ and the sarcolemmal Ca pump as $I_{pump} = I_{maxpump}([Ca]_i/([Ca]_i + K_{mpump}))$, with K_{mpump} = 0.5 μM and $I_{maxpump}$ = 0.038 A/F). G_{Cabkg} was adjusted to maintain a resting $[Ca]_i$ of 100 nM at −100 mV (3.2 S/F). Membrane capacitance was set to the average value observed in ferret myocytes (C_m = 173 pF), and the cytoplasmic volume was calculated using the species-specific conversion factor 7.96 pF/pl (Satoh et al., 1996). $[Ca]_o$ and $[Na]_o$ were fixed at 2 and 140 mM, respectively. $[Ca]_i$ and $[Na]_i$ were allowed to vary, and were initialized at 0.1 and 7 mM, respectively. $[Na]_i$ = 7 mM (Table II) was chosen based on the averages of fits to the ferret data. The total [Ca] increment for each Δt was defined by the following equation:

$$\Delta[Ca]_{total} = \frac{\int_t^{t+\Delta t}\left(I_{NCX} - \frac{I_{pump}}{2} - \frac{I_{Cabkg}}{2}\right)}{F \cdot \text{Volume myoplasm}}. \quad (2)$$

$[Ca]_{total}$ was converted to $[Ca]_i$ for every time step taking into account intrinsic cellular buffering (Hove-Madsen and Bers, 1993) as well as buffering by indo-1:

$$[Ca^{2+}]_{total} = [Ca^{2+}]_i + \frac{215}{1 + \frac{0.42}{[Ca^{2+}]_i}} + \frac{705}{1 + \frac{79}{[Ca^{2+}]_i}} + \frac{50}{1 + \frac{0.75}{[Ca^{2+}]_i}}. \quad (3)$$

The $[Na]_i$ increment for each Δt was defined by the following equation:

$$\Delta[Na]_i = \frac{-\int_t^{t+\Delta t} I_{NCX}}{3F \cdot \text{Volume}}, \quad (4)$$

in which Volume was the myoplasmic volume.

Data Acquisition and Analysis

Currents, fluorescence signals, and contraction data were recorded using PClamp6.4 and PClamp8 software (Axon Instruments). Data were analyzed using customized software written in Microsoft Visual Basic 6 and Microsoft Visual Basic for Applications, using Gigasoft ProEssentials Scientific Graphing Routines (www.gigasoft.com). Curve fits of the data to the equation for I_{NCX} were performed using the Majestic™ (Logix Consulting, Inc.) add-in for Microsoft Excel. Means and standard deviations of curve fit parameters are presented.

RESULTS

As described in MATERIALS AND METHODS, we blocked all currents other than I_{NCX} (including $I_{Cl}(Ca)$, $I_{Ca}(L)$, and the Na/K pump) as well as SR function. Thereafter, we regarded Ni-sensitive currents like that in Fig. 2 C as I_{NCX}. Thus, we have the fortunate situation that only I_{NCX} has the ability to bring Ca into and out of the cell. We control I_{NCX} directly using our voltage protocols.

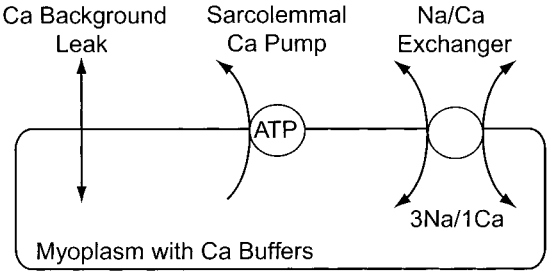

FIGURE 1. Computer model of cardiac myocyte containing nonblocked sources of Ca flux, used in Fig. 8. Ca background leak current is defined by constant conductance and electrochemical driving force for Ca, Ca pump follows Michaelis-Menten kinetics, and I_{NCX} is defined by Eq. 1.

TABLE II

Simulation Parameters Used in Fig. 8

	Ca activation	No Ca activation
K_{mCaAct}*	125	NA
V_{max} (A/F)	22.6	13.7
$[Na]_i$‡	7.16	7.10
G_{Cabkg} (S/F)	3.2	5.1

Parameters used in the computer simulation (Fig. 8) NA, not applicable. K_{mCaAct}, V_{max}, and $[Na]_i$ were based on fits to ferret data with and without the allosteric factor (Allo). G_{Cabkg} adjusted to give resting $[Ca]_i$ = 100 nM. Fixed parameters are listed in MATERIALS AND METHODS (see *Simulations and Calculations*).

*Values are measured in nanomolar.

‡Values are measured in millimolar.

Fig. 2 shows a representative record where the response to the same pulse protocol was recorded once in the absence (Fig. 2 A) and once in the presence (Fig. 2 B) of 10 mM Ni to reveal Ni-sensitive difference current, I_{NCX} (Fig. 2 C). With the Ni present, the current was relatively small and constant; correspondingly, the cell failed to contract with Ni present (compare bottom panels of Fig. 2, A and B).

Fig. 2 C shows how we established that Ca activation occurred. In the absence of allosteric regulation, the electrochemical effect of increasing $[Ca]_i$ would be to increase inward I_{NCX} but to decrease outward I_{NCX}. Ca activation, on the other hand, would increase I_{NCX} in both directions. Thus, we looked closely for changes in outward I_{NCX} since allosteric regulation opposes electrochemical regulation. Increases in outward I_{NCX} can only be attributed to allosteric regulation.

Fig. 3 (top, Measured) shows an example of the fluo-3 $[Ca]_i$ signal measured from a mouse myocyte overexpressing canine NCX1 superimposed with a prediction of $[Ca]_i$ based on integration of the recorded I_{NCX} (Fig. 3 top, Predicted). In this example, the duty factor of outward versus inward I_{NCX} was 25% (Fig. 3, bottom). As represented by the first term of Eq. 2, we calculated cumulative $[Ca]_{total}$ from the integrated I_{NCX}, using the fixed 3:1 Na/Ca I_{NCX} stoichiometry, and estimated myoplasmic volume (34 pl, based on 13.0 pF/pl cytosol for rat; Satoh et al., 1996). We used a standard cytosolic Ca buffering relationship (Hove-Madsen and Bers, 1993; Eq. 3) to solve for $[Ca]_i$ at each time point (Fig. 3 top, Predicted). The prediction corresponds reasonably well with $[Ca]_i$ measured using fluo-3. This provides additional support that the currents we were measuring are indeed I_{NCX}.

Fig. 4 A is an example record from a ferret myocyte (n = 22) that shows direct evidence of Ca activation at physiological $[Ca]_i$. Notice that the magnitude of outward and inward I_{NCX} both increase with rising $[Ca]_i$. The increase in outward I_{NCX} represents Ca activation. It is not due to the change in electrochemical potential because increasing $[Ca]_i$ decreases the driving force for allosteric Ca influx via outward I_{NCX}. The increase in inward I_{NCX} represents the combined electrochemical and allosteric effects of increasing $[Ca]_i$.

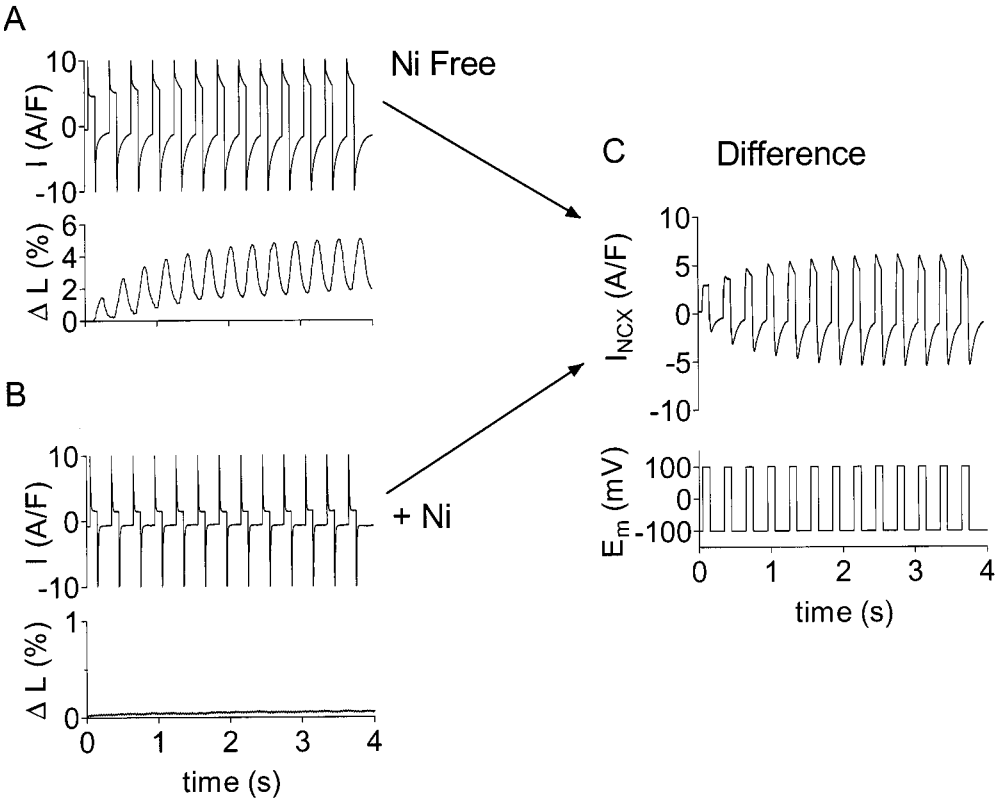

FIGURE 2. Protocol used to show regulation of I_{NCX} by $[Ca]_i$. K currents, I_{Cl}(Ca), I_{Ca}(L), Na/K pump, SR Ca pump blocked. (A) Current and contraction with application of alternating voltage clamp protocol in transgenic mouse myocyte overexpressing canine NCX1. B is the same as A, but with 10 mM Ni present. (C, top) Current in A minus current in B, which represents I_{NCX}. (C, bottom) Alternating voltage clamp protocol applied to the cell: +100 mV for 100 ms and −100 mV for 200 ms.

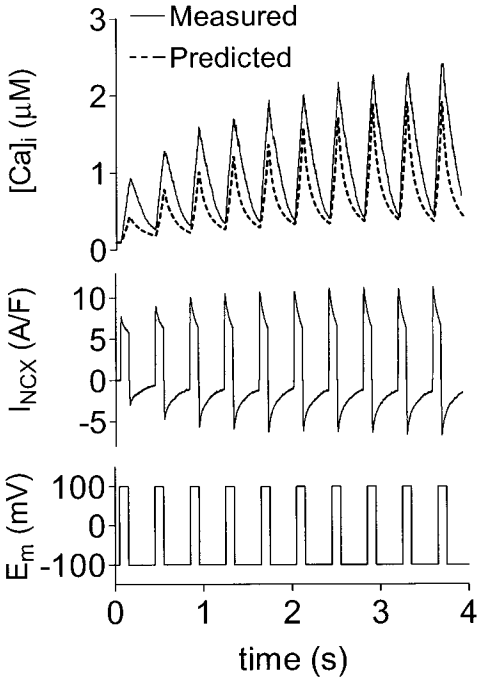

FIGURE 3. (Top) $[Ca]_i$ predicted using integral of I_{NCX} compares well with $[Ca]_i$ measured using fluo-3; mouse overexpressing normal canine NCX1. Total Ca (defined by Eq. 2) was converted to $[Ca]_i$ using Eq. 3. (Middle) I_{NCX} measured in absence of Ni and leak subtracted. (Bottom) Voltage protocol.

Fig. 4 B shows an example record made with the same protocol from a WT mouse myocyte ($n = 10$). Of the 10 records obtained from WT mouse myocytes, only one appeared to show any sign of allosteric Ca regulation (an increase of outward I_{NCX}). In 9/10 experiments, the outward I_{NCX} decreased. As expected from the purely electrochemical effects of increasing $[Ca]_i$, the inward I_{NCX} increased, although not dramatically in mice (see Fig. 7). Notably, mouse myocytes generally showed less inward I_{NCX} when compared with ferret (see Fig. 6). Fig. 4 C shows the response of a mouse myocyte overexpressing canine NCX1 to the alternating pulse protocol ($n = 7$). There were dramatic increases in both outward and inward I_{NCX}, which, as we noted above, is strong evidence of allosteric Ca regulation. Fig. 4 D illustrates the same protocol applied to a mouse myocyte overexpressing the Δ680-685 mutant of canine NCX1 ($n = 8$). Deleting these amino acids clearly eliminated the increase in outward I_{NCX} we attribute to allosteric Ca regulation. In every experiment, outward I_{NCX} decreased similarly as in WT mouse myocytes. Again, inward I_{NCX} still increased because of electrochemical considerations.

In Fig. 3, the outward and inward currents decline considerably during respective individual pulses. Such declines in the outward direction were minimal in most of our data (see examples in Fig. 4), especially in ferret

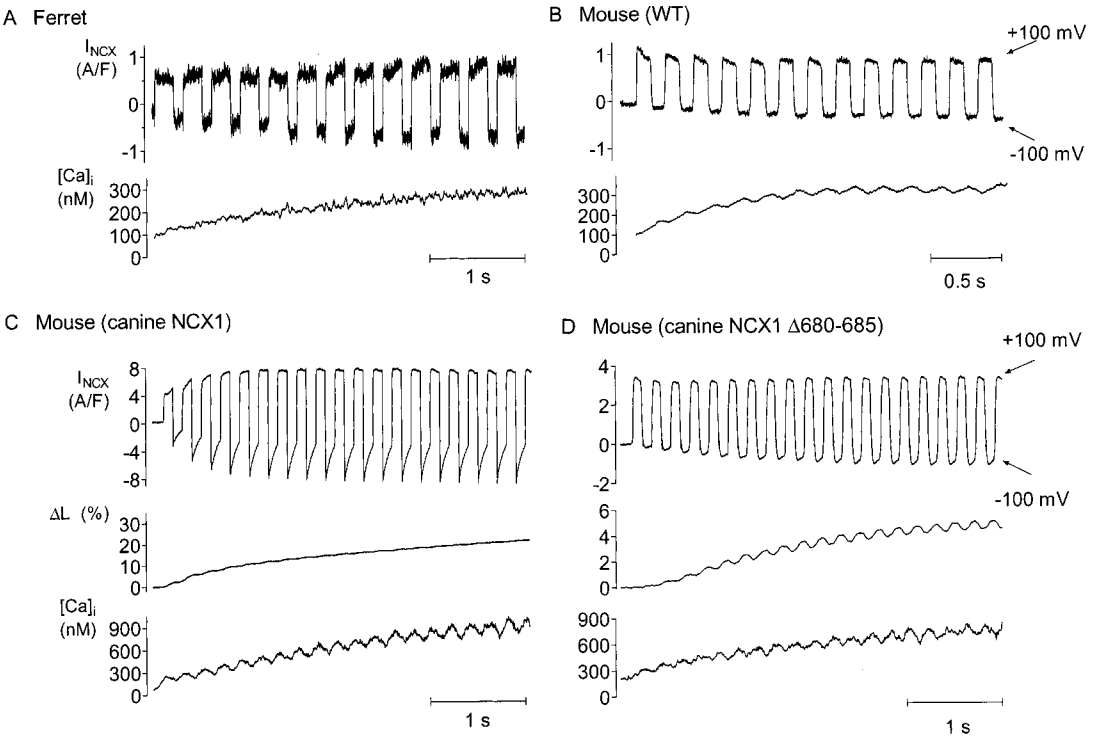

FIGURE 4. Examples of I_{NCX} in response to voltage protocol for four cell types studied. (A) Ferret myocyte showed Ca activation of I_{NCX} (top, Ni-sensitive I_{NCX}; bottom, $[Ca]_i$ measured using indo-1). (B) WT mouse myocyte. I_{NCX} did not show Ca activation (top, Ni-sensitive I_{NCX}; bottom, $[Ca]_i$ measured using fluo-3). (C) Mouse myocyte overexpressing canine NCX1 showed Ca activation of I_{NCX} (from top to bottom: Ni-subtracted I_{NCX}, percent contraction, and $[Ca]_i$ measured using fluo-3). (D) Mouse myocyte overexpressing Δ680-685 canine NCX1 did not show Ca activation (from top to bottom: leak-subtracted I_{NCX}, percent contraction, and $[Ca]_i$ measured using fluo-3).

myocytes. We attribute these declines to transient changes in $[Ca]_i$ and $[Na]_i$ during the overall increase in $[Ca]_i$ in a protocol (see Fig. 8). Declines in inward I_{NCX} were also pronounced in mouse myocytes expressing canine NCX, and this may be attributable to the combined effects of $[Ca]_i$ acting at allosteric and transport sites.

Data like those of Fig. 4 of each experiment where $[Ca]_i$ was measured were fit to Eq. 1 with and without the allosteric factor. Fig. 5 A shows fits of I_{NCX} versus $[Ca]_i$ for all the ferret myocytes where $[Ca]_i$ was measured (14/22). As noted in MATERIALS AND METHODS, each of the individual data points for the fit (symbols) was defined by I_{NCX} and $[Ca]_i$ time averaged over the duration of a particular voltage step. For the purpose of displaying the data only, I_{NCX} is shown normalized to its values at high $[Ca]_i$. For ferret (and mouse + canine NCX1), the fit to Eq. 1 with the allosteric term was better in every case ($P < 0.05$ by F test described in MATERIALS AND METHODS). K_m for allosteric Ca regulation was close to $[Ca]_{rest}$ (Ferret K_{mCaAct} = 125 ± 16 nM SEM). In contrast, data from the 6 (out of 10) WT mouse myocytes where $[Ca]_i$ was available were not fit better (or even as well) with the allosteric factor, with the exception of one cell, in which K_{mCaAct} was 49 nM, well below physiological $[Ca]_i$ (data not shown). Both fits of I_{NCX} versus $[Ca]_i$ in mice expressing canine NCX1 were better with the allosteric term (K_{mCaAct} = 158 or 418 nM, n = 2; data not shown). Since WT mouse myocytes do not show Ca activation over the range of $[Ca]_i$ studied (Fig. 4), the situation is simplified, and we can attribute the observed allosteric regulation to purely canine NCX1. Fig. 5 B shows fits of I_{NCX} versus $[Ca]_i$ in the Δ680-685 mice where $[Ca]_i$ was available (3/8). None of these fits was improved by including the allosteric factor, verifying that amino acids 680–685 play a role in Ca regulation of canine NCX1 expressed in mouse myocytes. Fit parameters for the four cell types studied are shown in Table I.

Fig. 6 shows the magnitudes of I_{NCX} at high $[Ca]_i$ for the four myocyte types studied. I_{NCX} at +100 mV was larger in ferret than WT mouse (2.47 vs. 1.48 A/F), but was increased three- to fourfold in transgenic mice (6.90 and 5.23 A/F). Where measured directly, the maximum $[Ca]_i$ attained was (mean ± SEM [in nM]): 257 ± 73 in WT mouse (n = 6); 254 ± 36 in ferret (n = 14); and, in accordance with the larger I_{NCX}, 861 and 765 in two mouse cells overexpressing canine NCX1, and 1,357 ± 613 in mouse overexpressing canine NCX1 Δ680-685 (n = 3). The severalfold larger outward I_{NCX} seen for both transgenic mouse models in this figure confirm the expected overexpression of canine NCX in comparison to NCX of WT mouse and ferret. Allosteric activation is nearly complete at these high $[Ca]_i$, and so this factor has no influence here. The change of the electrochemical factor with increasing $[Ca]_i$ does not contribute to the increase of outward I_{NCX} (in fact, this factor decreases slightly; see Fig. 10). Thus, the large outward I_{NCX} in the transgenic mice is evidence of upregulation of I_{NCX}.

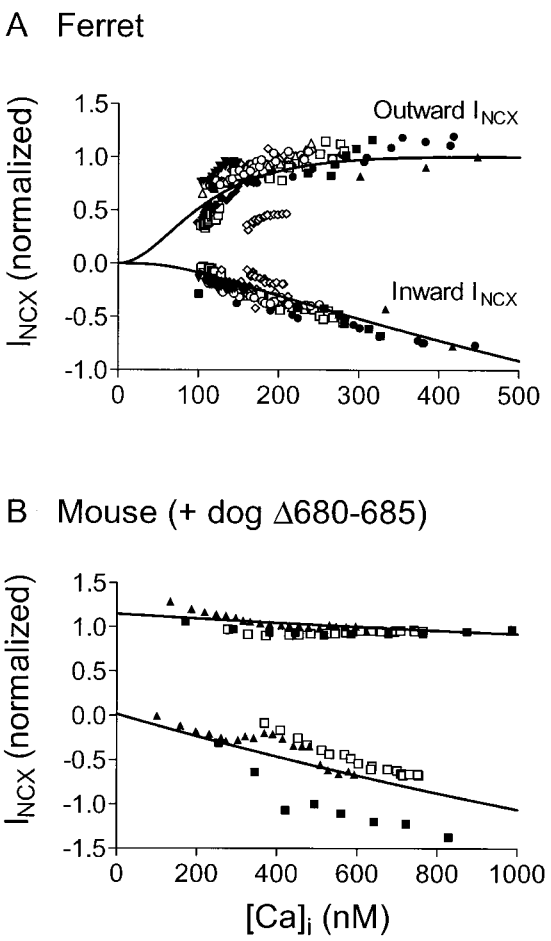

FIGURE 5. I_{NCX} versus $[Ca]_i$ fit to Eq. 1. (A) Solid lines show outward and inward I_{NCX} predicted from fits to the ferret data including the allosteric factor (K_{mCaAct} = 125 nM). Data of all 14 cells were less well fit ($P < 0.05$) when the allosteric factor was not included. (B) Solid lines show outward and inward I_{NCX} predicted from fits to data of mouse myocytes overexpressing Δ680-685 canine NCX1 without the allosteric factor. Including the allosteric factor did not improve the fits. Each symbol in A and B represents time-averaged I_{NCX} during a particular voltage step at the corresponding averaged $[Ca]_i$. For clarity, the figure shows data normalized to the fit predictions at $[Ca]_i$ = 500 nM in A and $[Ca]_i$ = 1,000 nM in B.

Fig. 7 shows summary data for the increment of I_{NCX} with increasing $[Ca]_i$ in all four NCX types studied. In the outward direction, I_{NCX} increased in ferret and in mouse myocytes expressing canine NCX1, but decreased in WT mouse and in mouse myocytes expressing the Δ680-685 deletion mutant of canine NCX1. Inward I_{NCX} always increased with increasing $[Ca]_i$, as would be expected even in the absence of Ca activation because of the increased inward electrochemical driving force, but the largest increases were in the ferret and the mouse overexpressing normal canine NCX1. These are the two preparations where Ca activation

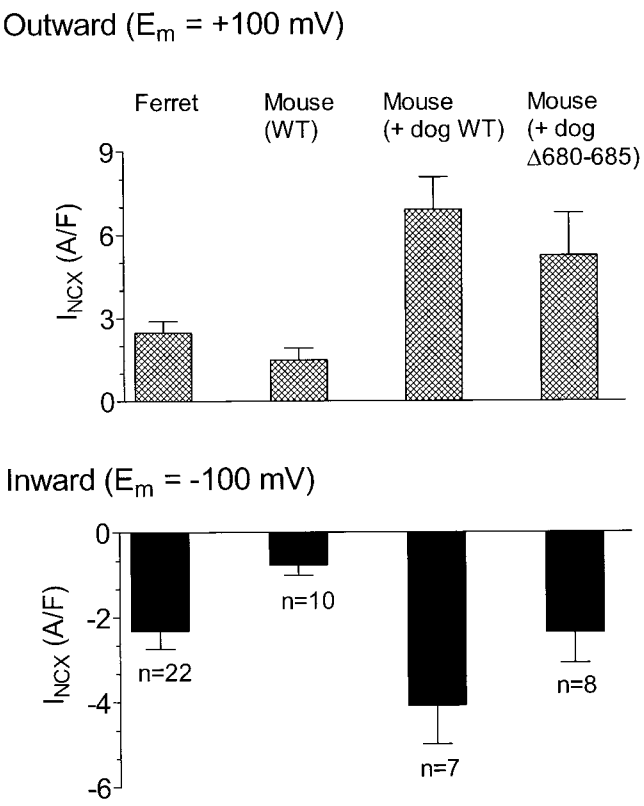

FIGURE 6. Magnitudes of I_{NCX} at high $[Ca]_i$ for the four NCX types studied. (Top) Outward I_{NCX} at +100 mV; (bottom) inward I_{NCX} at −100 mV. Data are means ± SEM of the currents recorded during the final pulses of the corresponding alternating protocols.

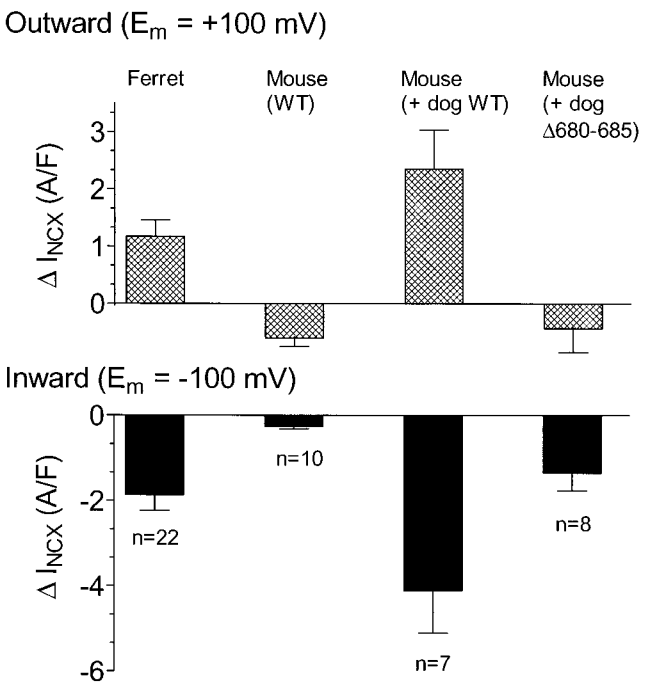

FIGURE 7. Among the four preparations studied, only those with Ca activation of I_{NCX} showed increasing outward and dramatically increasing inward I_{NCX} with increasing $[Ca]_i$. (Top) Outward I_{NCX} at +100 mV; (bottom) inward I_{NCX} at −100 mV. Currents are taken as the difference between the first pulse (at low $[Ca]_i$) and the last pulse (at high $[Ca]_i$). Data are means ± SEM.

would be expected to cause additional increase in I_{NCX} beyond the electrochemical component.

We have shown in Fig. 7 the absolute increment in I_{NCX} density without normalization to the initial I_{NCX} density. In all cases, we attempted to choose a voltage protocol that brought I_{NCX} to a maximally activated state. Accordingly, we did not adjust these data for the particular amount of $[Ca]_i$ increase. Thus, in this summary figure, we were able to include experiments where we did not record $[Ca]_i$, as long as we had contraction records consistent with large increases in $[Ca]_i$.

Fig. 8 A shows simulated I_{NCX} in response to our alternating voltage protocol (Fig. 8 G) as predicted using Eq. 1, with allosteric Ca regulation included (K_{mCaAct} = 125 nM). Fig. 8 E (bold trace) shows $[Ca]_i$ as defined by Eq. 2. V_{max} and $[Na]_i$ were determined from fits of the ferret data (Fig. 5 A) with the Ca regulatory term (Table II). Fig. 8 (B, D, F, and H) shows I_{NCX}, $[Na]_i$, $[Ca]_i$, and E_m, respectively, for an early and late pulse of Fig. 8 A. Note that during the first few pulses, the outward I_{NCX} increased during 100 ms at +100 mV (because of allosteric activation; Fig. 8 B, a). However during later pulses, outward I_{NCX} was relatively flat, and even started to decline slightly (Fig. 8 B, b). This is explained by a 71-μM decrease in $[Na]_i$ (Fig. 8 D) and a corresponding 132- nM increase in $[Ca]_i$ (Fig. 8 F), resulting in decreases in ΔE of 4 and 3%, respectively, while this decline in ΔE was countered almost exactly by a 7% increase in allosteric factor over the same increase in $[Ca]_i$. This spectrum of behavior reflects reasonably well the behavior of I_{NCX} recorded experimentally where allosteric regulation was apparent (Fig. 2 C and Fig. 4, A and C).

Fig. 8 C shows the same simulation for I_{NCX} without Ca regulation, and the corresponding $[Ca]_i$ is shown in Fig. 8 E (thin trace). V_{max} and $[Na]_i$ were determined from fits of the ferret data without the Ca regulatory term (Table II). There is a decline in the outward I_{NCX} envelope when no allosteric regulation is considered (by 8.8%) and this matches the observations in WT mouse and mouse overexpressing Δ680-685 canine NCX1 (Fig. 4, B and D). This decline is due to the electrochemical effect of the rising $[Ca]_i$ and declining $[Na]_i$, as described above, which in this case (unlike Fig. 8 A), are not offset by an increasing allosteric factor. Thus, the simple model provides a reasonable description of both the current envelope, and also describes changes within individual pulses.

To test how rapidly Ca activation of outward I_{NCX} occurs, we induced a rapid and steady-state increase in $[Ca]_i$ from ~100 nM to ~1 μM (Fig. 9). In this case, thapsigargin was omitted and the SR was preloaded

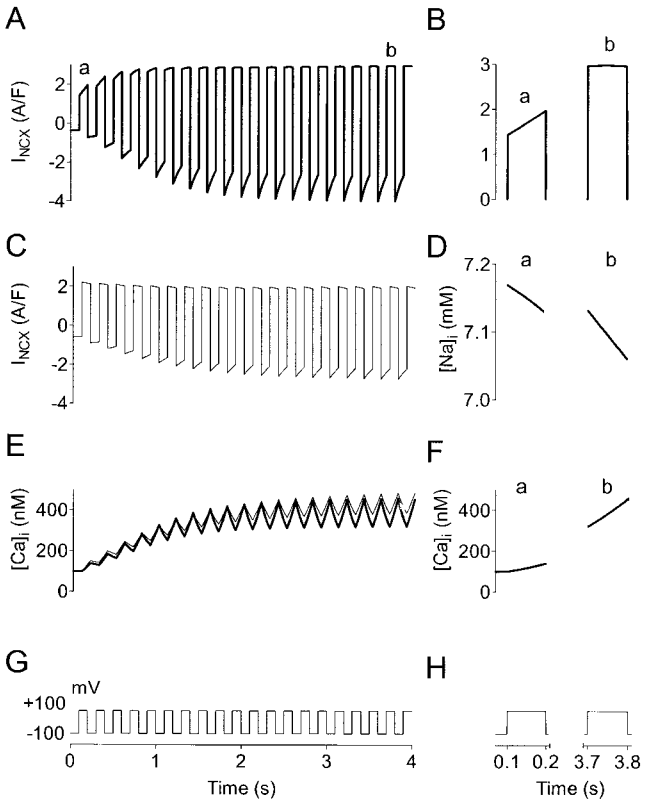

FIGURE 8. Computer simulations based on model in Fig. 1. (A, bold trace) I_{NCX} with Ca activation (Eq. 1, K_{mCaAct} = 125 nM). Both outward and inward I_{NCX} grow as $[Ca]_i$ increases in response to alternating protocol. (B) Outward I_{NCX} during single pulses, early (a) and late (b) of A. (C, thin trace) I_{NCX} (Eq. 1 with allosteric factor omitted). Without Ca activation, outward I_{NCX} declines slightly while inward I_{NCX} increases less dramatically. (D) $[Na]_i$ time course for pulses B (a and b). (E) $[Ca]_i$ time course with (bold trace) and without (thin trace) Ca activation. (F) $[Ca]_i$ time course for pulses B (a and b). (G) Voltage protocol was identical for all simulations. (H) Voltage for pulses B (a and b). In all simulations, Ca background leak density (G_{Cabkg}) was adjusted to give initial resting $[Ca]_i$ = 100 nM at −100 mV. Simulation parameters based on fits to the ferret data are given in Table II. Other parameters not based on our experiments are given in MATERIALS AND METHODS.

with Ca by outward I_{NCX}. Depolarization from −100 to +100 mV caused an initial slow rise in $[Ca]_i$ and outward I_{NCX}. Abrupt exposure to 10 mM caffeine induced a rapid rise in $[Ca]_i$ (τ = 61 ms), and this caused a nearly parallel increase in outward I_{NCX} (τ = 40 ms) without any appreciable time lag. Although this does not define an explicit time constant for I_{NCX} activation, it makes our simplifying assumption of instantaneous regulation reasonable. Moreover, the rapidity of activation of Na/Ca exchange suggests that regulation may occur on a beat to beat basis.

DISCUSSION

We have examined intact cardiac myocytes from four different sources (WT ferret and WT mouse, as well as two transgenic mouse models) for allosteric Ca regulation of I_{NCX} at physiological $[Ca]_i$. We used a protocol in which the activating Ca was alternately brought into the cell via outward I_{NCX} at +100 mV, and extruded via inward I_{NCX} at −100 mV (Fig. 2). By varying the periods at ±100 mV (in the range of 100–300 ms), we were able to control and measure the rate of growth in $[Ca]_i$ while simultaneously measuring both inward and outward I_{NCX}. In ferret myocytes, the outward and inward I_{NCX} both increased with increasing $[Ca]_i$ (Figs. 4 and 7). We attribute the increasing outward I_{NCX} to Ca activation, which has predominance over the reduction in electrochemical gradient for Ca to enter the cell. The electrochemical gradient would otherwise decrease outward I_{NCX}. In contrast to the increase in outward I_{NCX} that we always saw in ferret myocytes, WT mouse outward I_{NCX} decreased in all but 1 out of 10 experiments (although inward I_{NCX} still increased; Figs. 4 B and 7). Additionally, in the absence of Ca activation, inward I_{NCX} increased to a smaller extent (Fig. 7, mouse versus ferret).

We also investigated allosteric Ca regulation in mouse myocytes overexpressing canine NCX1 (Fig. 4 B). The rationale behind experiments with transgenic mice was two-fold. First, we wanted to determine if canine NCX overexpressed in mice would show allosteric regulation like the ferret NCX. Figs. 4 B and 7 illustrate that outward I_{NCX} did increase with increasing $[Ca]_i$, indicating that canine NCX has similar Ca activation properties to ferret NCX (for outward I_{NCX}, ΔI_{NCX}/final I_{NCX} represented an increase of 38 ± 12% SEM [n = 7] in canine versus 41 ± 4% SEM [n = 22] in ferret). Second, since mutant canine NCX lacked Ca-dependent regulation of outward I_{NCX} in giant membrane patch studies (Maxwell et al., 1999), a comparison of I_{NCX} between these two types of transgenic myocytes overexpressing canine NCX should help verify that the increase in outward I_{NCX} was due to allosteric regulation and not some other process.

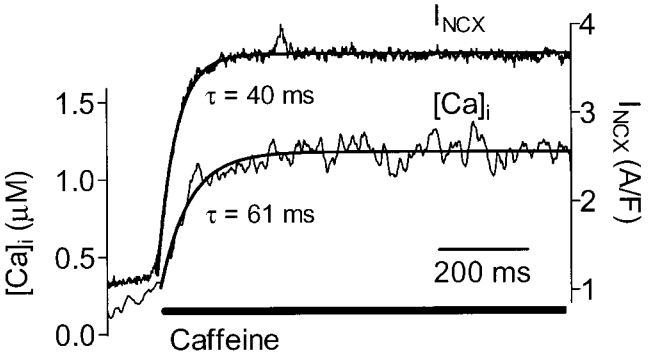

FIGURE 9. Rapid time course of development of Ca activation in ferret myocyte. Caffeine was applied at +100 mV to cause rapid increase in $[Ca]_i$. There was no apparent delay between the activation of outward I_{NCX} and the rise in $[Ca]_i$. Solutions were identical to those described in MATERIALS AND METHODS, but pretreatment with thapsigargin- and caffeine-containing solutions was omitted.

Figs. 4 D, 5 B, and 7 show that deletion of this putative Ca regulatory region eliminated the increase in outward I_{NCX} in our protocol. This deletion made the canine I_{NCX} look very much like WT mouse I_{NCX}, with the exception that its magnitude was severalfold larger (Fig. 6).

Fig. 10 A shows how the predicted allosteric activation (Allo) and electrochemical factors (ΔE) in Eq. 1 would contribute to increasing outward and inward I_{NCX} (Allo · ΔE) as $[Ca]_i$ increases up to 500 nM. In the outward direction, I_{NCX} is largely dominated by the Allo factor, whereas in the inward direction, the Allo factor and ΔE factors both contribute. For this figure, the $[Ca]_i$-dependent allosteric and electrochemical factors in Eq. 1 were predicted using the averages of the respective parameters fit to the 14 sets of ferret data, and are shown normalized to their values at 500 nM $[Ca]_i$. From the predictions, we can infer the respective experimentally observed final values of $[Ca]_i$ the relative contributions of allosteric activation and electrochemical driving force. In ferrets, outward I_{NCX} increased by 67% from its initial value as $[Ca]_i$ rose from 115 ± 9 nM (SEM) to 254 ± 36 nM (SEM). This was mainly due to a 75% increase in the allosteric factor, offset slightly by a 4% decrease in the electrochemical factor (1.75 × 0.96 = 1.67). Inward I_{NCX} in ferret increased by 283% with this $[Ca]_i$ increase. The allosteric factor increased by the same 75%, but in this case it was complemented by a 119% increase in the electrochemical factor, resulting in the final effect (1.75 × 2.19 = 3.83). Thus, the allosteric and electrochemical factors contribute nearly equally to the increase in inward I_{NCX} recorded in ferret.

Fig. 10 B shows the effects of $[Na]_i$ on the electrochemical factor of Eq. 1 at $[Ca]_i$ = 100 and 500 nM. Changes in $[Na]_i$ (in the millimolar range) are not expected to occur rapidly, but species-dependent variations in $[Na]_i$ do occur. $[Na]_i$ appears to be substantially elevated in mouse myocytes relative to nonmurids (7.2 in rabbit and 12.7 in rat [Shattock and Bers, 1989]; 14-17 mM in mouse [Yao et al., 1998]). This is also suggested by the results of our fits (Table I), and this may account for the small inward I_{NCX} in mouse (Fig. 4, B–D, and Fig. 6).

Our simulations (Fig. 8) also predict that I_{NCX} drives micromolar changes in $[Na]_i$ within pulses during our oscillatory protocols. Referring to outward I_{NCX}, during the final 100-ms pulse to +100 mV in Fig. 8 B, b, declining $[Na]_i$ (Fig. 8 D) and increasing $[Ca]_i$ (Fig. 8 F) contribute about equally to declines in ΔE (see RESULTS), and this, combined with allosteric activation by Ca, results in the relatively flat current during the pulse. However, the relatively flat relationship between ΔE and $[Na]_i$ for inward I_{NCX} (Fig. 10 B), coupled with the steep dependence of inward I_{NCX} on $[Ca]_i$, at −100 mV makes inward I_{NCX} relatively insensitive to changing $[Na]_i$. Changing $[Na]_i$ alone, within the range observed in Fig. 8, causes less than a 1% decline in inward

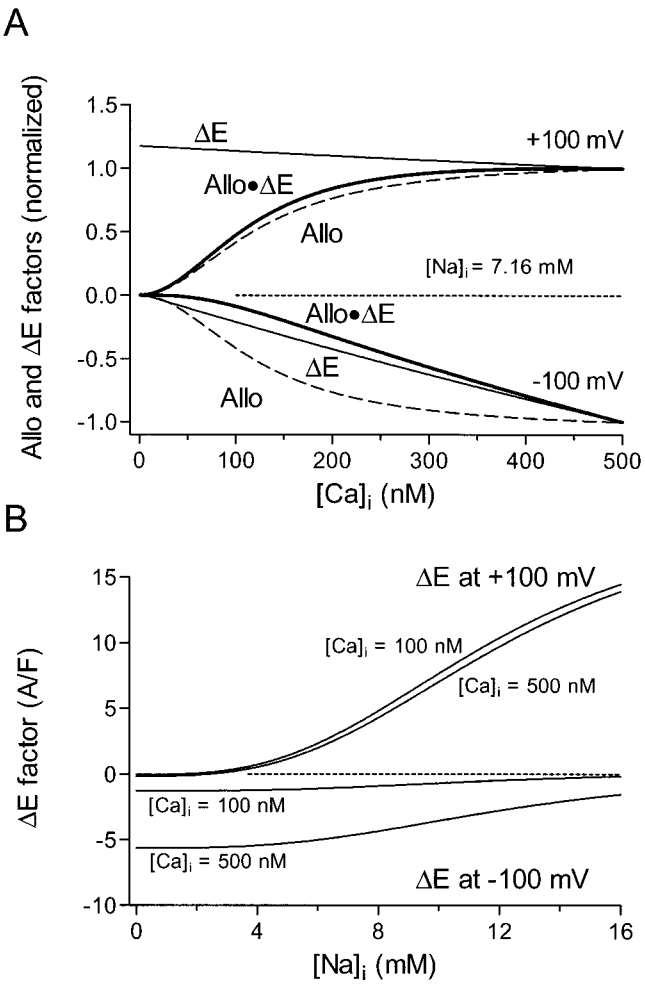

FIGURE 10. Allosteric (Allo) and electrochemical (ΔE) contributions to ferret I_{NCX} (see Eq. 1). (A) In the outward direction, the increase of I_{NCX} is dominantly due to the Allo factor, whereas in the inward direction, the Allo factor and ΔE factors both contribute. Factors have been normalized to their values at $[Ca]_i$ = 500 nM. (B) Effects of $[Na]_i$ on variations in ΔE at $[Ca]_i$ = 100 and 500 nM. In the outward direction, changes in $[Na]_i$ and $[Ca]_i$ contribute approximately equally to changing ΔE, however, ΔE in the inward direction is dominated by changes in $[Ca]_i$. ΔE not normalized here.

I_{NCX}, and almost all of the within-pulse changes in inward I_{NCX} are due to changing $[Ca]_i$, acting either electrochemically or allosterically.

Measurement of I_{NCX}

There is no inhibitor that is selective for I_{NCX} without affecting other currents; accordingly, we approached this problem by blocking all currents other than I_{NCX} with their appropriate inhibitors (as well as by ion substitution). We took I_{NCX} as either the difference current before versus after applying Ni or the current remaining after analytical leak subtraction. Two additional observations support the idea that the currents we recorded are I_{NCX}. Fig. 6 shows that I_{NCX} is indeed larger in the NCX overexpressing myocytes compared with

I_{NCX} in WT mouse myocytes (compare raw currents in Fig. 4 B with those in Fig. 2 and Fig. 4, C and D). Further, the time course of $[Ca]_i$ calculated using I_{NCX} and known cytosolic buffering characteristics (Eq. 3) predicted the measured $[Ca]_i$ rather well (Fig. 3).

Nonselective Ca-activated currents have been reported in ventricular myocytes (Colquhoun et al., 1981) at micromolar $[Ca]_i$. In rabbits (Schlotthauer and Bers, 2000), virtually all current evoked by Ca release was I_{NCX} and/or Ca-activated Cl current. In ferret (Ginsburg et al., 1998), all Ca-activated inward current is abolished by the replacement of Na_o with Li (which should still allow this nonselective current to flow). Furthermore, in the present experiments, Ni blocked both outward and inward I_{NCX}, but is not expected to inhibit Ca-activated nonselective cation current (Niggli, 1989).

Comparison to Earlier Studies

We have shown for the first time allosteric regulation in intact myocytes at physiological $[Ca]_i$, and under conditions where the NCX is able to dynamically control $[Ca]_i$. Miura and Kimura (1989), in intact guinea pig myocytes, showed Ca regulation with $[Ca]_i$ artificially held well below the normal resting $[Ca]_i$ (K_{mCaAct} = 22 nM). They found a steep Ca dependence (n_{Hill} = 3.7) and concluded that I_{NCX} was maximally activated when $[Ca]_i$ reached 50 nM. A similar low K_{mCaAct}, 44 nM (n_{Hill} = 1.6), was found by Fang et al. (1998) for the bovine cardiac NCX expressed in Chinese hamster ovary cells. Maxwell et al. (1999) showed Ca activation of WT mouse NCX in giant membrane patches between 0 and 3 μM (but no values were obtained between 0 and 1 μM [Ca]). It is conceivable that our failure to observe Ca regulation of WT mouse I_{NCX} (as described by Maxwell et al., 1999) is due to a low intrinsic K_{mCaAct} in mouse (comparable to the 22–44 nM values above), and lower than we observe in the ferret or dog NCX; i.e., mouse NCX may be fully activated at diastolic $[Ca]_i$ of 100 nM. Indeed, the only WT mouse myocyte whose I_{NCX} versus $[Ca]_i$ fit was actually improved with the Ca regulatory term, showed activation with an apparent K_{mCaAct} = 49 nM. At 100 nM resting $[Ca]_i$, this would imply 82% activation (for n_{Hill} = 2 or 95% for n_{Hill} = 4), in contrast to 39% activation at 100 nM $[Ca]_i$ in the ferret (for n_{Hill} = 2). Thus, since we did not explore subphysiological $[Ca]_i$, intrinsic Ca regulation in the mouse could have escaped our detection. On the other hand, this made mouse myocytes a convenient background in which to study transgenic overexpression of canine NCX with respect to Ca regulation at physiological $[Ca]_i$ (since the endogenous mouse NCX may always be fully activated).

Our K_{mCaAct}, 125 nM in the ferret, although only somewhat larger numerically, would result in maximal sensitivity of I_{NCX} to changes in $[Ca]_i$ near $[Ca]_{rest}$. The disparity between previous results and ours, as well as our finding of a functional difference between the ferret and WT mouse, indicate that there are species and/or preparation-dependent differences in the regulation of I_{NCX} by $[Ca]_i$. For example, EGTA can increase the apparent [Ca] dependence of NCX in sarcolemmal vesicles (Trosper and Philipson, 1984), which could have produced underestimates of K_{mCaAct} in earlier work. An interesting side point is that the NCX of *Drosophila melanogaster*, calx, although regulated by $[Ca]_i$ in the 100-nM range, shows inactivation, not activation, with increasing $[Ca]_i$ (Hryshko et al., 1996).

Species dependency does not explain why Hilgemann et al. (1992) observed K_{mCaAct} to be 0.3–0.6 μM in giant excised patches, 10 times higher than Miura and Kimura (1989) reported, and 2 to 4 times as high as our value. Both studies used guinea pig myocytes. Either preparation, Ca buffering, or washout of other factors might explain these differences. Our study differs from all previous approaches, not only in using intact myocytes, which probably retain key regulatory components, but also in allowing dynamic $[Ca]_i$ regulation.

We have noted (Fig. 8) that $[Na]_i$ and $[Ca]_i$ can vary transiently during the overall increase of $[Ca]_i$ in our protocol, possibly explaining the declines in I_{NCX} within pulses (Fig. 3). In connection with these variations, subsarcolemmal [Ca] may have reached higher values than our fluorescence-based $[Ca]_i$ measurements indicated. Then, we would have underestimated K_{mCaAct}. However, we fit K_{mCaAct} using only ferret data, and these data had very little within-pulse I_{NCX} variation.

Physiological Relevance

A reduction in I_{NCX} at low $[Ca]_i$ may limit the ability of outward I_{NCX} to trigger SR Ca release during the upstroke of an action potential (Noble et al., 1991). During diastole, deactivation of inward I_{NCX} may help maintain the SR Ca load by shifting the Ca flux balance away from sarcolemmal Ca extrusion and towards the SR. Deactivation of I_{NCX} may help prevent resting $[Ca]_i$ from going much below threshold for myofilament activation (Fabiato, 1983). Additionally, the probability of $[Ca]_i$ to trigger SR Ca release is a steep function that depends on the square of local $[Ca]_i$ near the ryanodine receptors (Santana et al., 1996; Cheng et al., 1996). Thus, small variations in NCX activity may fine tune resting $[Ca]_i$ and, in doing so, may help to define the threshold necessary for Ca to trigger the opening of the SR release channels (Litwin et al., 1998). Finally, since NCX normally works to extrude Ca as $[Ca]_i$ increases, Ca activation may reduce the likelihood of Ca overload (unless $[Na]_i$ gets very high).

We have assumed a stoichiometry of 3:1 Na:Ca in this paper (Reeves and Hale, 1984; Kimura et al., 1987), however, Fujioka et al., (2000) recently reported a stoichiometry closer to 4:1 Na/Ca, so that for every net charge

transferred by the flow of I_{NCX}, 1/2 Ca ion rather than 1 Ca ion is transferred in the opposite direction. A 4:1 NCX would tend to draw $[Ca]_i$ to 130 pM at E_{rest} rather than 38 nM for a 3:1 NCX (−80 mV, 10 mM $[Na]_i$, 140 mM $[Na]_o$, 2 mM $[Ca]_o$, 37°C). In the prediction of Fig. 3, a 4:1 stoichiometry would also reduce the Ca flux inferred from I_{NCX} by a factor of 2 and leave it insufficient to explain $\Delta[Ca]_i$. Although further evaluation of the proposed 4:1 stoichiometry is needed, if true, then deactivation of I_{NCX} at low $[Ca]_i$ would be even more crucial to prevent diastolic $[Ca]_i$ from falling far too low.

If mean $[Ca]_i$ is elevated, as may occur at high heart rates or during heart failure (Gwathmey et al., 1987), the average state of NCX activity may be elevated. If this is the case, and the NCX functions predominantly in the Ca efflux mode, Ca activation may serve as a negative feedback mechanism that helps to prevent Ca overload and spontaneous SR Ca release. On the other hand, since I_{NCX} is thought to be a major component of the transient inward current (Fedida et al., 1987; Lipp and Pott, 1988; Schlotthauer and Bers, 2000), Ca activation may actually promote delayed afterdepolarizations with spontaneous SR release. Furthermore, if $[Na]_i$ rises to high enough levels (e.g., submembrane space or digitalis toxicity), Ca influx is favored electrochemically and, in this case, Ca activation could worsen Ca overload.

Model

We chose to fit an instantaneous model because experiments in intact cells do not allow the fast homogenous cytoplasmic solution changes needed to study the dynamics of Ca activation precisely. There may be a lag between the [Ca] in the vicinity of the NCX and the bulk $[Ca]_i$ measured by fluorescent indicators (Trafford et al., 1995), which is not included in our model. Since we cannot distinguish spatial and temporal $[Ca]_i$ heterogeneities from activation kinetics, we have chosen to model Ca activation as an instantaneous process. Our simulation of the ferret data (Fig. 8) with allosteric Ca regulation modeled in this manner matched well with the characteristic growing outward envelope of I_{NCX} and also with changes during individual pulses. Furthermore, we found no delay in activation of I_{NCX} when a rapid release of SR Ca was used to cause $[Ca]_i$ to increase from 100 to >1 μM (Fig. 9). This might be related to Baazov et al. (1999), who found very rapid activation, although Kappl and Hartung (1996) indicated an activation time constant of 620 ms. Rapid activation, along with K_{mCaAct} = 125 nM, suggests that variation in Ca activation might be relevant in beat-to-beat regulation of I_{NCX}. Indeed, the $[Ca]_i$ dependence of inward I_{NCX} reflects a composite of both K_{mCai} and K_{mCaAct}, and the apparent linearity often reported may be serendipitous.

The primary aim of this study was to determine if allosteric regulation of the NCX played a role in the intact cell under conditions where $[Ca]_i$ changed within a physiological range. We conclude that allosteric Ca-dependent activation of I_{NCX} occurs in ferret myocytes and in mouse myocytes overexpressing dog NCX1. We also confirm that amino acids 680–685 are important for Ca regulation, since regulation did not occur in mouse myocytes overexpressing canine NCX1 lacking this region. Under our experimental conditions and $[Ca]_i$ range, Ca activation did not occur in WT mouse myocytes (contrast Maxwell et al., 1999). Although this lack of Ca regulation in the WT mouse may be condition-dependent, we speculate that it may be due to species differences in amino acid sequences within NCX1. Although NCX1 is ~99% identical between mouse and dog, a difference does occur within the 680–685 region (IIEESY in dog versus IIQESY in mouse; Nicoll et al., 1990; Nicoll and Philipson, 1991).

We thank Dr. Donald W. Hilgemann for stimulating discussions and Drs. Jeanne Nerbonne, Weinong Guo, and Haodong Xu for their help with our development of mouse myocyte preparations. We also thank Steve Scaglione and Sarah Wimbiscus for their help with the ferret myocyte isolations.

This work was supported by the National Institutes of Health grants R01HL-30077DMB, R01-HL64098DMB, R01-HL48509KDP, and AHA Fellowship 0010180ZCRW.

Submitted: 3 August 2000
Revised: 17 November 2000
Accepted: 13 December 2000

REFERENCES

Adachi-Akahane, S., L. Lu, Z. Li, J.S. Frank, K.D. Philipson, and M. Morad. 1997. Calcium signaling in transgenic mice overexpressing cardiac Na^+/Ca^{2+} exchanger. *J. Gen. Physiol.* 109:717–729.

Baazov, D., Z. Wang, and D. Khananshvili. 1999. Time-resolved monitoring of electrogenic Na^+-Ca^{2+} exchange in the isolated cardiac sarcolemma vesicles by using a rapid-response fluorescent probe. *Biochemistry.* 38:1435–1445.

Bassani, J.W.M., R.A. Bassani, and D.M. Bers. 1995. Calibration of indo-1 and resting intracellular $[Ca]_i$ in intact rabbit cardiac myocytes. *Biophys. J.* 68:1453–1460.

Bers, D.M. 1991. Excitation-contraction coupling and cardiac contractile force. Kluwer Academic Publishers, The Netherlands. 258 pp.

Cheng, H., W.J. Lederer, and M.B. Cannell. 1993. Calcium sparks: elementary events underlying excitation-contraction coupling in heart muscle. *Science.* 262:740–744.

Cheng, H., M.R. Lederer, W.J. Lederer, and M.B. Cannell. 1996. Calcium sparks and $[Ca^{2+}]_i$ waves in cardiac myocytes. *Am. J. Physiol.* 270:C148–C159.

Colquhoun, D., E. Neher, H. Reuter, and C.F. Stevens. 1981. Inward current channels activated by intracellular Ca in cultured cardiac cells. *Nature.* 294:752–754.

Coulombe, A., I.A. Lefevre, I. Baro, and E. Coraboeuf. 1989. Barium- and calcium-permeable channels open at negative membrane potentials in rat ventricular myocytes. *J. Membr. Biol.* 111:57–67.

Fabiato, A. 1983. Calcium-induced release of calcium from the cardiac sarcoplasmic reticulum. *Am. J. Physiol.* 245:C1–C14.

Fang, Yu, M. Condrescu, and J.P. Reeves. 1998. Regulation of the Na^+/Ca^{2+} exchange activity by cytosolic Ca in transfected Chinese hamster ovary cells. *Am. J. Physiol.* 275:C50–C55.

Fedida, D., D. Noble, A.C. Rankin, and A.J. Spindler. 1987. The arrhythmogenic transient inward current i_{ti} and related contraction in isolated guinea-pig ventricular myocytes. *J. Physiol.* 392:523–542.

Fujioka, Y., M. Komeda, and S. Matsuoka. 2000. Stoichiometry of Na^+-Ca^{2+} exchange in inside-out patches excised from guinea-pig ventricular myocytes. *J. Physiol.* 523:339–351.

Ginsburg, K.S., C.R. Weber, and D.M. Bers. 1998. Control of maximum sarcoplasmic reticulum Ca load in intact ferret ventricular myocytes. Effects of thapsigargin and isoproterenol. *J. Gen. Physiol.* 111:491–504.

Grynkiewicz, G., M. Poenie, and R.Y. Tsien. 1985. A new generation of Ca indicators with greatly improved fluorescence properties. *J. Biol. Chem.* 260:3440–3450.

Gwathmey, J.K., L. Copelas, R. MacKinnon, F.J. Schoen, M.D. Feldman, W. Grossman, and J.P. Morgan. 1987. Abnormal intracellular calcium handling in myocardium from patients with end-stage heart failure. *Circ. Res.* 61:70–76.

Haworth, R.A., and A.B. Goknur. 1991. Control of the Na-Ca exchanger in isolated heart cells. II. Beat-dependent activation in normal cells by intracellular calcium. *Circ. Res.* 69:1514–1524.

Hilgemann, D.W. 1990. Regulation and deregulation of cardiac Na^+-Ca^{2+} exchange in giant excised sarcolemmal membrane patches. *Nature.* 344:242–245.

Hilgemann, D.W., A. Collins, and D.P. Cash. 1991. Cardiac Na^+-Ca^{2+} exchange system in giant membrane patches. *Annu. NY Acad. Sci.* 639:127–139.

Hilgemann, D.W., A. Collins, and S. Matsuoka. 1992. Steady state and dynamic properties of cardiac sodium-calcium exchange: secondary modulation by cytoplasmic calcium and ATP. *J. Gen. Physiol.* 100:933–961.

Hove-Madsen, L., and D.M. Bers. 1993. Passive Ca buffering and SR Ca uptake in permeabilized rabbit ventricular myocytes. *Am. J. Physiol.* 264:C677–C686.

Hryshko, L., S. Matsuoka, D.A. Nicoll, J.N. Weiss, E.M. Schwarz, S. Benzer, and K.D. Philipson. 1996. Anomalous regulation of the *Drosophila* Na^+-Ca^{2+} exchanger by Ca^{2+}. *J. Gen. Physiol.* 108:67–74.

Kappl, M., and K. Hartung. 1996. Rapid charge translocation by the cardiac Na^+-Ca^{2+} exchanger after a Ca concentration jump. *Biophys. J.* 71:2473–2485.

Kimura, J., S. Miyamae, and A. Noma. 1987. Identification of sodium-calcium exchange current in single ventricular cells of guinea-pig. *J. Physiol.* 384:199–222.

Levitsky, D.O., D.A. Nicoll, and K.D. Philipson. 1994. Identification of the high affinity Ca-binding domain of the cardiac Na^+-Ca^{2+} exchanger. *J. Biol. Chem.* 269:22847–22852.

Lipp, P., and L. Pott. 1988. Transient inward current in guinea-pig atrial myocytes reflects a change of sodium-calcium exchange current. *J. Physiol.* 397:601–630.

Litwin, S.E., J. Li, and J.H.B. Bridge. 1998. Na-Ca exchange and the trigger for sarcoplasmic reticulum Ca release: studies in adult rabbit ventricular myocytes. *Biophys. J.* 75:359–371.

Luo, C.-H., and Y. Rudy. 1994. A dynamic model of the cardiac ventricular action potential: I. simulations of ionic currents and concentration changes. *Circ. Res.* 74:1071–1096.

Matsuoka, S., D.A. Nicoll, R.F. Reilly, D.W. Hilgemann, and K.D. Philipson. 1993. Initial localization of regulatory regions of the cardiac sarcolemmal Na^+-Ca^{2+} exchanger. *Proc. Natl. Acad. Sci. USA.* 90:3870–3874.

Matsuoka, S., D.A. Nicoll, L.V. Hryshko, D.O. Levitsky, J.N. Weiss, and K.D. Philipson. 1995. Regulation of the cardiac Na^+-Ca^{2+} exchanger by Ca: mutational analysis of the Ca binding domain. *J. Gen. Physiol.* 105:403–420.

Maxwell, K., J. Scott, A. Omelchenko, A. Lukas, L. Lu, Y. Lu, M. Hnatowich, K.D. Philipson, and L.V. Hryshko. 1999. Functional role of ionic regulation of Na^+/Ca^{2+} exchange assessed in transgenic mouse hearts. *Am J. Physiol.* 277:H2212–H2221.

Miura, Y., and J. Kimura. 1989. Sodium-calcium exchange current: dependence on internal Ca and Na and competitive binding of external Na and Ca. *J. Gen. Physiol.* 93:1129–1145.

Mullins, L.J. 1979. The generation of electric currents in cardiac fibers by Na/Ca exchange. *Am. J. Physiol.* 236:C103–C110.

Nicoll, D.A., and K.D. Philipson. 1991. Molecular studies of the cardiac sarcolemmal sodium-calcium exchanger. *Annu. NY Acad. Sci.* 639:181–188.

Nicoll, D.A., S. Longoni, and K.D. Philipson. 1990. Molecular cloning and functional expression of the cardiac sarcolemmal Na^+-Ca^{2+} exchanger. *Science.* 250:562–565.

Niggli, E. 1989. Strontium-induced creep currents associated with tonic contractions in cardiac myocytes isolated from guinea-pigs. *J. Physiol.* 414:549–568.

Noble, D., S.J. Noble, G.C.L. Bett, Y.E. Earm, W.K. Ho, and I.K. So. 1991. The role of sodium-calcium exchange during the cardiac action potential. *Proc. Natl. Acad. Sci. USA.* 639:334–353.

Pogwizd, S.M., M. Qi, W.-L. Yuan, A.M. Samarel, and D.M. Bers. 1999. Upregulation of Na/Ca exchanger expression and function in an arrhythmogenic rabbit model of heart failure. *Circ. Res.* 85:1009–1019.

Reeves, J.P., and C.C. Hale. 1984. The stoichiometry of the cardiac sodium-calcium exchange system. *J. Biol Chem.* 259:7733–7739.

Santana, L.F., H. Cheng, A.M. Gomez, M.B. Cannell, and W.J. Lederer. 1996. Relation between the sarcolemmal Ca^{2+} current and Ca^{2+} sparks and local control theories for cardiac excitation-contraction coupling. *Circ. Res.* 78:166–171.

Satin, J., and L.L. Cribbs. 2000. Identification of a T-type Ca^{2+} channel isoform in murine atrial myocytes (AT-1 cells). *Circ. Res.* 86: 636–642.

Satoh, H., L.M. Delbridge, L.A. Blatter, and D.M. Bers. 1996. Surface:volume relationship in cardiac myocytes studied with confocal microscopy and membrane capacitance measurements: species-dependence and developmental effects. *Biophys. J.* 70:1494–1504

Schlotthauer, K., and D.M. Bers. 2000. Sarcoplasmic reticulum Ca^{2+} release causes myocyte depolarization: underlying mechanism and threshold for triggered action potentials. *Circ. Res.* 87:774–780.

Segel, I.H. 1993. Enzyme Kinetics. Behavior and Analysis of Rapid Equilibrium and Steady-state Enzyme Systems. John Wiley & Sons, Inc., New York. 957 pp.

Shattock, M.J., and D.M. Bers. 1989. Rat vs. rabbit ventricle: Ca flux and intracellular Na assessed by ion-selective microelectrodes. *Am. J. Physiol.* 256:C813–C822.

Trafford, A.W., M.E. Díaz, S.C. O'Neill, and D.A. Eisner. 1995. Comparison of subsarcolemmal and bulk calcium concentration during spontaneous calcium release in rat ventricular myocytes. *J. Physiol.* 488:577–586.

Trosper, T.L., and K.D. Philipson. 1984. Stimulatory effect of calcium chelators on Na^+-Ca^{2+} exchange in cardiac sarcolemmal vesicles. *Cell Calcium.* 5:211–222.

Weber, C.R., K.S. Ginsburg, and D.M. Bers. 1999. Calcium activation of the sodium calcium exchanger in intact cardiac myocytes. *Biophys. J.* 76:A299. (Abstr.)

Weber, C.R., K.S. Ginsburg, D.M. Bers, K.D. Philipson. 2000. Calcium activation of Na/Ca exchanger in mouse myocytes overexpressing canine NCX1. *Biophys. J.* 78:53A. (Abstr.)

Yao, A., Z. Su, A. Nonaka, I. Zubair, L. Lu, K.D. Philipson, J.H. Bridge, and W.H. Barry. 1998. Effects of overexpression of the Na^+-Ca^{2+} exchanger on $[Ca^{2+}]_i$ transients in murine ventricular myocytes. *Circ. Res.* 82:657–665.

Yuan, W., and D.M. Bers. 1995. Protein kinase inhibitor H-89 reverses forskolin stimulation of cardiac L-type calcium current. *Am. J. Physiol.* 268:C651–C659.